

ECE 445  
SENIOR DESIGN LABORATORY  
FINAL REPORT

---

# Airloom Type Vertical Axis Wind Turbine

---

**Team #38**

CHENGSHENG JIANG  
(jiang98@illinois.edu)

YIYANG ZHOU  
(yiyang27@illinois.edu)

JIAYI GUO (jiayig8@illinois.edu)

JIAYAO LIN  
(jiayaol3@illinois.edu)

TA: Yanbing Yang  
Professor: Jiahuan Cui

May 18, 2025

## Abstract

This report presents the development of an elliptical lift-type Vertical Axis Wind Turbine (VAWT), which aims at enhancing energy conversion efficiency and reducing construction costs. The project focus on improving the performance of VAWTs, which traditionally suffer from lower efficiency and high structural costs. The proposed solution integrates a mechanical module with blades arranged in an elliptical configuration to optimize aerodynamic performance, and a control module featuring an STM32 microcontroller for real-time monitoring, a boost converter circuit for voltage regulation, and a Maximum Power Point Tracking (MPPT) algorithm to maximize power output.

Key innovations include the use of 3D-printed components to lower costs and a reconstructed HTD 5M tooth profile to mitigate mechanical inefficiencies such as tooth skipping. Computational Fluid Dynamics (CFD) simulations validated the design, with an eight-bladed configuration achieving a mechanical power output of 185 W at a tip speed ratio (TSR) of 2. The system also incorporates safety and ethical considerations, adhering to IEEE standards for electrical safety and environmental sustainability.

The total project cost was maintained under 1,500 yuan, with a detailed schedule ensuring timely completion. The results demonstrate the potential of this VAWT design to contribute to renewable energy solutions by balancing efficiency and reliability.

# Contents

<b>1</b>	<b>Introduction</b>	<b>1</b>
1.1	mechanical module . . . . .	1
1.2	control module . . . . .	1
1.3	performance requirements . . . . .	2
<b>2</b>	<b>Design</b>	<b>3</b>
2.1	Design Procedure . . . . .	3
2.1.1	Aerodynamic Energy Capture . . . . .	3
2.1.2	Support Frame and Power Transmission . . . . .	4
2.2	Design Details . . . . .	4
2.2.1	Blade and Aerodynamic Design . . . . .	4
2.2.2	Pulley-Belt System . . . . .	5
2.2.3	Aluminum Profile Base Design . . . . .	7
2.2.4	Fixation of the Rotating Shaft . . . . .	7
2.2.5	DC Motor Mounting . . . . .	8
2.2.6	Generator Pulley-Belt System . . . . .	8
2.2.7	Boost and Converter circuit . . . . .	9
2.3	Charging control . . . . .	11
2.3.1	interrupt . . . . .	12
<b>3</b>	<b>Verification</b>	<b>14</b>
3.1	Mechanical part . . . . .	14
3.2	Electronic part . . . . .	14
<b>4</b>	<b>Costs</b>	<b>15</b>
4.1	Cost . . . . .	15
4.2	Schedule . . . . .	16
<b>5</b>	<b>Conclusion</b>	<b>17</b>
	<b>References</b>	<b>18</b>
	<b>Appendix A Example Appendix</b>	<b>19</b>

# 1 Introduction

The global energy crisis demands innovative solutions to reduce dependence on fossil fuels while meeting rising energy needs. Wind energy is a sustainable and abundant resource, offering significant potential. However, the practical application of Vertical Axis Wind Turbines (VAWTs) still face many challenges in efficiency and scalability. Traditional VAWTs exhibit lower power output per unit and high structural costs, limiting their viability for utility-scale applications.

This project aims at addressing these limitations by developing an elliptical lift-type VAWT that enhances energy conversion efficiency while leveraging cost-effective manufacturing techniques. We divide the whole work into two different modules: the mechanical module and the control module as the following block diagram shows 1.

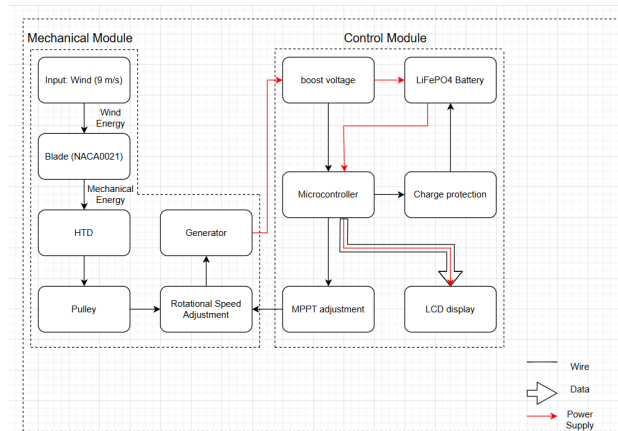


Figure 1: Airloom Type VAWT Flowchart

## 1.1 mechanical module

Mechanical Module is a square-airloom-type VAWT to convert wind energy to mechanical energy. In details, using NACA0021 blades, wind generates positive work on blades under certain angles[1]. Blades are fixed on the HTD. Moving HTD drives pulley to rotate. Shaft of Aluminum is fixed with pulley and gives torque to generator.

## 1.2 control module

This control module has two main functions, boost voltage in order while maximizing efficiency, and manage batter while displaying data.

For voltage boosting and maximizing efficiency part, We plan to use a development board named CBB24210 (based on the STM microcontroller and boost circuit) to guarantee a fixed voltage output (provisionally set at 48V). This development board features a relatively complete hardware configuration and a heat dissipation function, which can reduce design risks.

For battery management and data display part, we are using EV2759-Q-01A, a highly integrated switching charger designed for portable devices with 1- to 6-cell series Li ion or Li polymer battery packs as battery management since it is also equipped with a protection mechanism. And we want to use a 5.5 inch LCD display real-time charging current (0A to 10 A with  $\pm 0.5A$  accuracy), voltage (40V to 60 V for 48V batteries with  $\pm 0.5V$  accuracy), and battery state of charge (SOC) (0% to 100% with  $\pm 1\%$  accuracy).

### **1.3 performance requirements**

- With the wind speed of 9 m/s, tip speed ratio can reach 2 and VAWT can generate energy to charge the battery. Every component can bear the periodic force and be used for more than 1000h.
- The current rectification of the DC wind turbine generator will yield a fixed voltage output (provisionally set at 24V) which will be connected to the charging circuit. This circuit will use a boost circuit for voltage regulation and an MPPT algorithm to control the circuit output to enhance power generation efficiency.
- It must incorporate protection mechanisms to prevent overcharging, overdischarging, overcurrent, and overtemperature. In addition, the controller shall provide real-time monitoring of charging parameters, such as voltage and current via an LCD display, ensuring transparency and control over the charging process.

## 2 Design

### 2.1 Design Procedure

This section summarizes the top-level choices that shaped the Airloom-type vertical-axis wind-turbine (VAWT) prototype and explains why each was selected over plausible alternatives. Figure 1 (block diagram) groups the system into four interacting subsystems: aerodynamic energy capture, mechanical power transmission, electrical generation & power conditioning, and control/protection.

#### 2.1.1 Aerodynamic Energy Capture

The elliptical wind turbine operates with blades moving along an oval trajectory. Its key advantage lies in the enhanced relative wind velocity in the vertical direction at specific positions (as illustrated in Fig. 2)[2], which increases the blade's *lift-to-drag ratio*. This enhancement generates positive torque that converts wind energy into mechanical power.

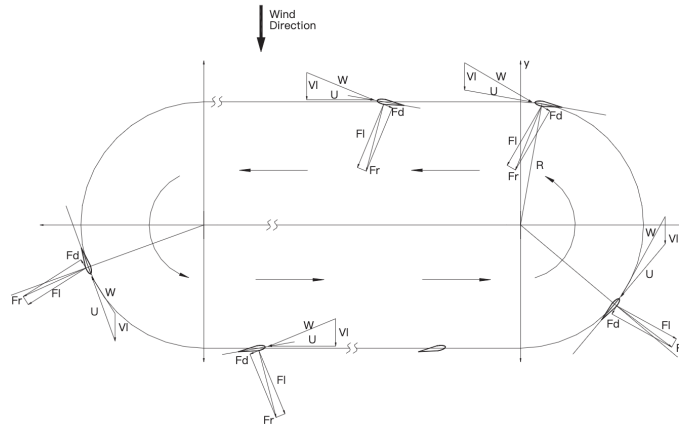


Figure 2: Energy generation/dissipation zones in elliptical VAWT operation. Red arrows indicate power-producing segments, blue shows energy-consuming regions.

However, during certain trajectory segments, the incoming wind actually *dissipates* mechanical energy from the blades. The system compensates by harvesting additional energy from other blade segments. Mathematically, the net power output  $P_{\text{net}}$  can be expressed as:

$$P_{\text{net}} = \oint_{\Gamma} \left( \vec{F}_{\text{lift}} + \vec{F}_{\text{drag}} \right) \cdot d\vec{s} \quad (1)$$

where  $\Gamma$  represents the oval trajectory. The efficiency improvement stems from:

- Increased vertical trajectory length (major axis) enhancing energy capture

- Reduced frontal area (minor axis) decreasing material usage compared to circular VAWTs with equivalent swept area
- Compact footprint requiring less installation space

### 2.1.2 Support Frame and Power Transmission

Alternatives Considered:

Welded elliptical steel ring track with blade carts and electromagnetic induction power take-off.

The stationary rail carries copper coils, and each blade cart carries a magnet array. Relative motion induces EMF (Faraday's law) to charge the battery.

Selected Solution:

Timing belt and pulleys with blades fastened directly to the belt.

Reason: Although the rail-and-cart concept offers lower running friction and greater structural stiffness and stability, fabricating the welded metal circular track is excessively difficult and far more expensive than the pulley-and-belt alternative. Also, the belt length can be easily adjusted for larger diameters; induction rail would require full re-winding.

Belt power transfer:

$$P = T v_b \eta_b$$

Where  $P$  is the power,  $T$  is the tension in belt,  $v_b$  is the belt operating speed and  $\eta_b$  is the pulley-belt efficiency.

Pulley Torque:

$$T_p = \frac{P}{\omega_p}$$

where  $T_p$  is the pulley torque,  $\omega_p$  is the angular velocity of the pulley, and  $P$  is the power.

## 2.2 Design Details

### 2.2.1 Blade and Aerodynamic Design

Figure 3a presents the CFD simulation results for a conventional vertical axis wind turbine design. The velocity contours reveal a well-defined wake region characterized by moderate flow deceleration (dark blue areas), corresponding to a power output of 97.59 W. This baseline configuration demonstrates typical aerodynamic behavior for this class of wind turbine.

The modified four-bladed square rotor configuration, illustrated in Figure 3b, exhibits enhanced flow interaction characteristics. The wake region shows increased flow deceleration and greater spatial extent compared to the conventional design, suggesting improved

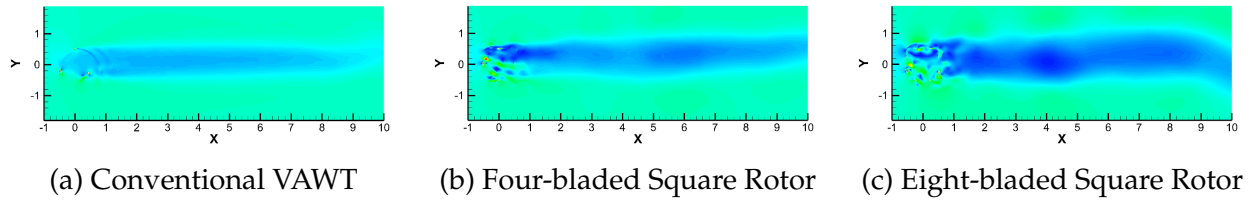


Figure 3: Computational fluid dynamics analysis of three VAWT configurations at TSR = 2, showing velocity field contours and wake structures

energy extraction capability. However, this configuration yielded a slightly lower power output of 88.28 W, indicating potential areas for optimization in blade geometry.

Most notably, the eight-bladed square rotor (Figure 3c) demonstrates superior performance characteristics. The extensive wake region and pronounced velocity reduction indicate efficient energy extraction from the airflow. Quantitative analysis confirms this observation, with the configuration generating 185 W of mechanical power - approximately double the output of the conventional design. This significant performance improvement led to its selection as the primary configuration for subsequent development phases.

Experimental measurements revealed substantial frictional losses in the system:

$$\tau_{\text{friction}} = \tau_{\text{rotor-base}}(2\text{ N}) + \tau_{\text{belt-pulley}}(1.8\text{ N}) + \tau_{\text{interference}}(2.3\text{ N}) \quad (2)$$

where  $\tau_{\text{interference}}$  occurs probabilistically when belt fasteners engage with pulley teeth. This 6N cumulative friction created a starting torque threshold that exceeded our initial design specifications. Through iterative testing, we determined that increasing the blade count to 12 provided sufficient starting torque to overcome these frictional forces while maintaining operational efficiency.

## 2.2.2 Pulley-Belt System

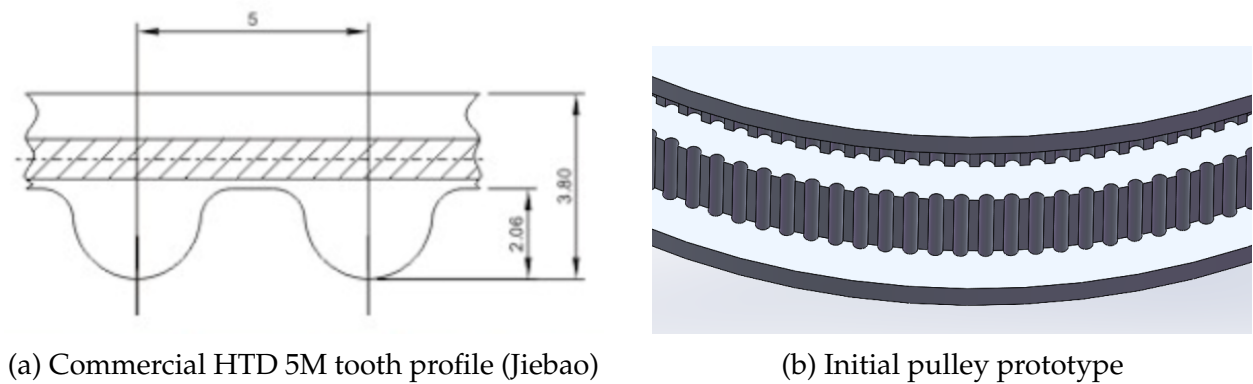


Figure 4: Initial timing belt transmission system components based on partial manufacturer specifications

The transmission system development began with analysis of commercial HTD tooth profiles provided by Ningbo Jiebao Power Transmission Systems Co., Ltd (Figure 4a[3]). Due to incomplete geometric specifications (particularly in the root region), our initial design approach focused on the available tooth tip geometry. The resulting pulley prototype (Figure 4b) featured 162 uniformly spaced holes arranged on a 128.75 mm pitch circle diameter, with each mounting point positioned at 2.98 mm radius for synchronous wheel applications.

Static testing indicated satisfactory belt engagement, with apparent proper meshing between pulley teeth and timing belt. However, dynamic operational testing revealed significant performance issues, including frequent tooth skipping and excessive frictional losses. These operational challenges were attributed to geometric mismatches in the incomplete tooth profile specification.

Further investigation confirmed that detailed HTD profile geometries are typically proprietary information. Available technical references, such as norelem[4], provide only basic dimensional parameters without complete construction details. To address this limitation, we developed an improved tooth profile model comprising three distinct geometric segments: a circular arc tooth tip, transitional straight flank, and root fillet arc, as shown in Figure 5a.

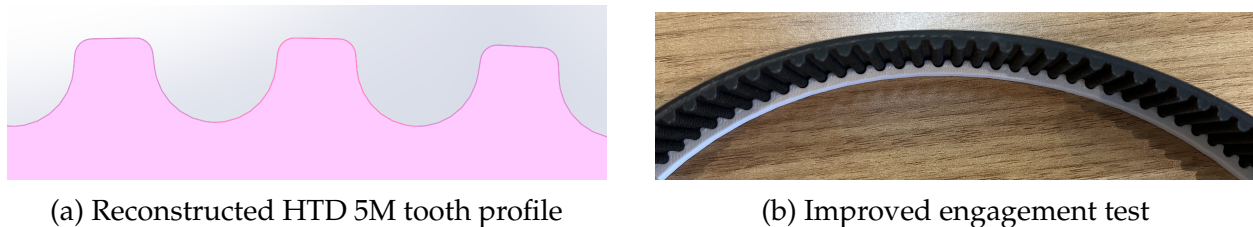


Figure 5: Optimized tooth profile design and validation testing

The reconstructed tooth profile was implemented in a 3D-printed prototype for experimental validation. Static fit tests (Figure 5b) demonstrated substantially improved belt-pulley engagement compared to the initial design. This successful verification establishes a foundation for ongoing dynamic performance evaluation, which will focus on identifying and resolving any residual tooth-skipping phenomena or abnormal friction under operational conditions.

During post-assembly testing, we observed imperfect gear meshing at junction points due to multiple error sources: 0.12mm 3D printing tolerance, approximately 0.3mm AB adhesive thickness, and outward expansion of outer teeth during fixation. With these errors accumulating across 84 teeth and manual visual alignment of upper/lower tooth rows, the final positional error reached 2 ~ 3 teeth, causing audible clicking noises and significantly increased friction during operation.

The solution involved complete redesign of an integrated pulley (Fig. 6) that directly connects the timing belt to the metal shaft, removing all intermediate attachment points that previously caused cumulative errors.

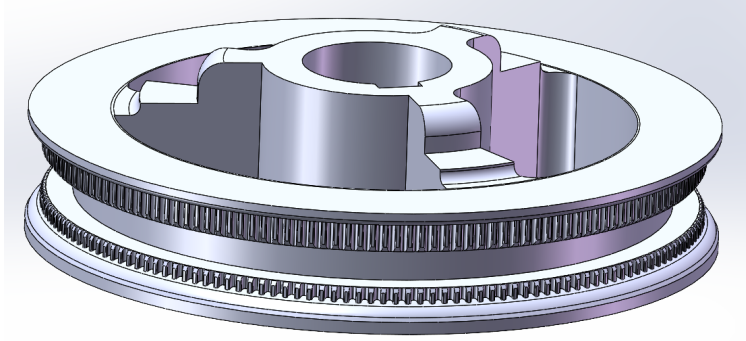


Figure 6: Redesigned integrated pulley for belt-to-shaft power transmission, eliminating alignment errors through monolithic construction

### 2.2.3 Aluminum Profile Base Design

The support frame (887.5 mm long, 887.5 mm wide, 360mm high) was constructed using 30x30 mm european standard aluminum extrusion profiles due to their high modularity, stiffness, and ease of assembly with 3-way connectors and corner brackets. This modular approach allows for future component adjustments and simplifies fabrication.

The frame is dimensioned to accommodate the rotational radius of the blade system and support axial loads transferred from the vertical axis blades.

### 2.2.4 Fixation of the Rotating Shaft

To ensure the stability and smooth operation of the elliptical rotating blade system, each vertical shaft is supported and constrained by two custom mounting bases spaced 300 mm apart vertically. These bases are connected to the aluminum profile frame through snap-fit joints that slide and lock into the T-slot channels, enabling precise alignment and robust mechanical support.

The shaft passes through two green radial ball bearings, which are press-fitted into the upper and lower mounting bases. These radial bearings are responsible for horizontal (radial) support, minimizing shaft deflection due to lateral forces from the blade motion or wind-induced vibrations.

To resist vertical loading from the blade weight and transmission torque, a blue thrust ball bearing is embedded in the bottom mounting block. This bearing provides axial support, significantly reducing vertical friction and ensuring that the shaft can rotate freely without excessive downward pressure on the radial bearings.

This dual-support configuration—radial bearings for lateral constraint and a thrust bearing for vertical load—ensures mechanical decoupling of forces, minimizes wear, and increases overall system stability during high-speed or long-duration operation.

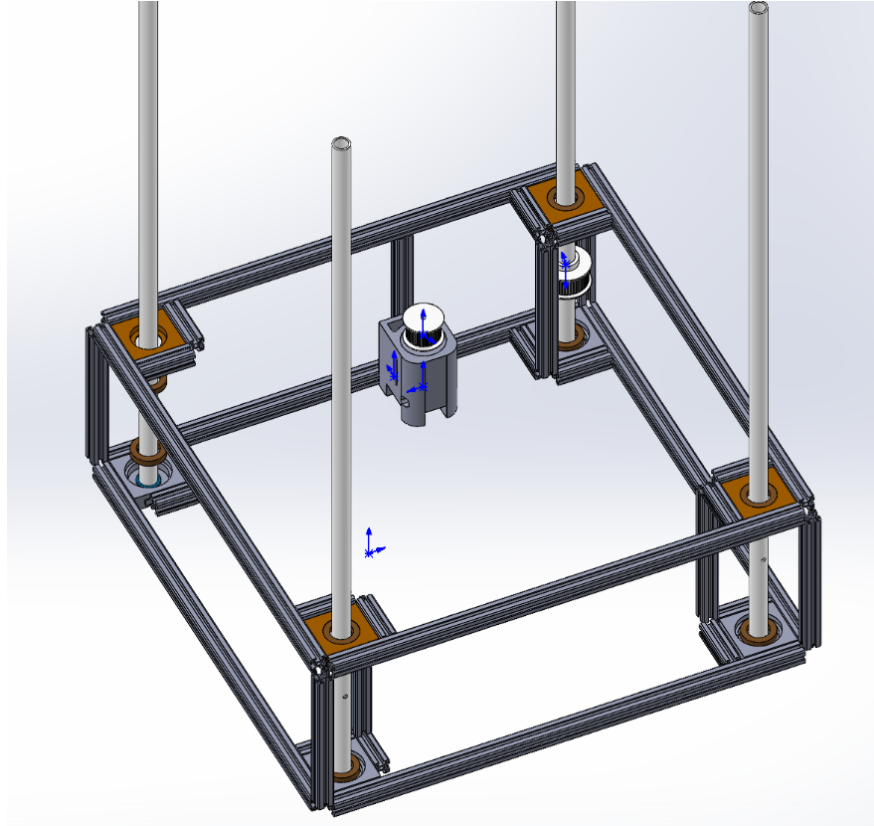


Figure 7: Aluminum Profile Base and Power Transmission System

### 2.2.5 DC Motor Mounting

The DC generator is mounted on the base using sliders and corner brackets that match the slot profiles, which allows the belt tension to be adjusted by sliding the motor mount along the aluminum profile and secured by corner brackets.

### 2.2.6 Generator Pulley-Belt System

The transmission system includes:

A large pulley ( $\Phi = 80$  mm) mounted on the selected rotating shaft.

A smaller pulley ( $\Phi = 60$  mm) attached to the generator shaft

A reinforced rubber timing belt (1m long, 30mm wide) for slip-free power transfer

### Pulley Diameter and Motor RPM Calculation

$$V_{\text{blade}} = \text{TSR} \cdot V_{\text{wind}} \quad [1]$$

$$\text{RPM}_{\text{axis}} = \frac{V_{\text{blade}}}{\pi \cdot \phi_{\text{blade pulley}}} \cdot 60 \quad [2]$$

$$\text{RPM}_{\text{motor}} = \text{RPM}_{\text{axis}} \cdot \frac{\phi_{\text{large}}}{\phi_{\text{small}}} \quad [3]$$

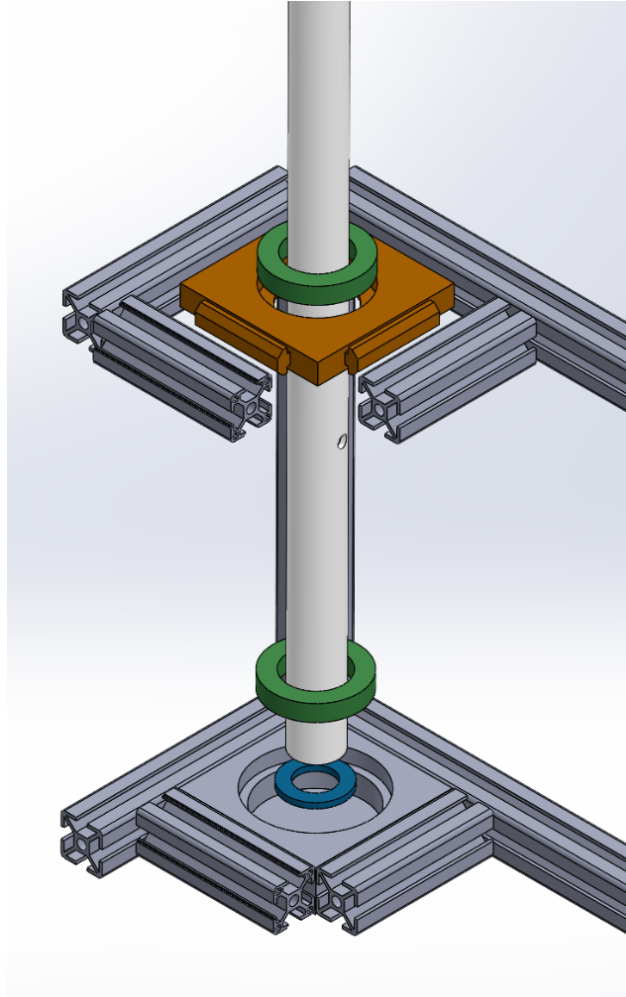


Figure 8: Shaft Fixation

Where TSR is the Tip Speed Ratio,  $V_{wind}$  is the wind speed,  $\phi_{blade\ pulley}$  is the Blade System Pulley Diameter,  $RPM_{motor}$  is the rpm of DC generator,  $RPM_{axis}$  is the rpm of the driving axis,  $\phi_{large}$  is the larger pulley mounted on the selected rotating shaft,  $\phi_{small}$  is the smaller pulley attached to the generator shaft.

Result:

$$RPM_{motor} = 1791.4$$

The rated power of the DC motor is 300W at 1500 - 2000 rpm, which meets the requirements.

### 2.2.7 Boost and Converter circuit

Serving as the energy source for the system, the selected 24V DC generator generates electrical energy driven by wind. The output voltage of the generator directly correlates with wind speed; as wind speed increases, the output voltage rises accordingly. Thus,

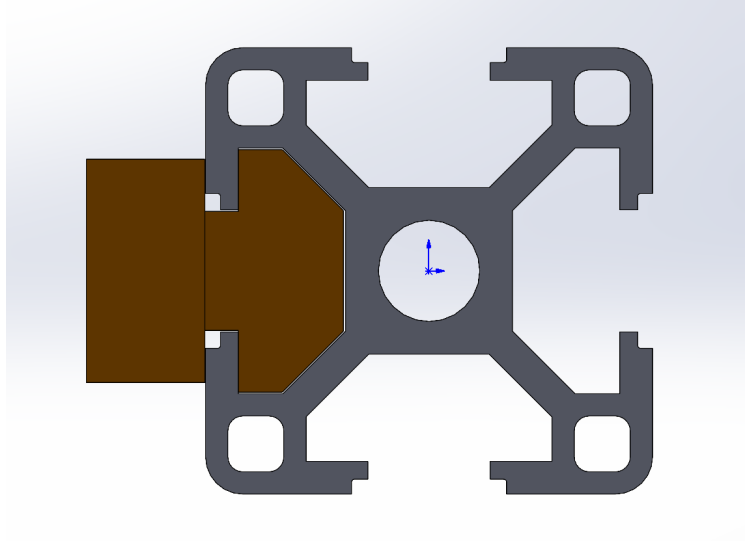


Figure 9: Slot Matching Mechanism

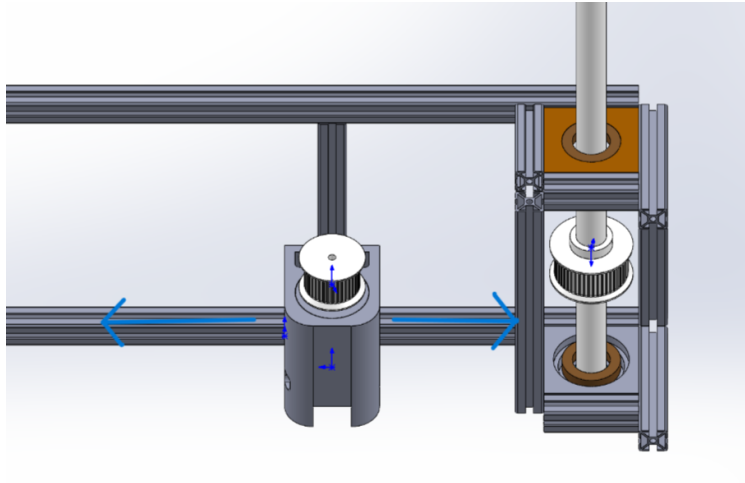


Figure 10: Sliding Schematic

the design must take into account the output characteristics of the generator to adapt to varying environmental conditions effectively.

To meet the charging requirements of the battery, a boost conversion circuit is designed. This component will elevate the 24V output voltage through PWM modulation and energy storage in inductors to a suitable charging voltage (e.g., 36V or higher) for various battery types (like lithium-ion or lead-acid). High-efficiency MOSFETs and appropriately sized inductors are selected to minimize power loss and thermal degradation.

Also, we implemented MPPT technology, which could continuously adjust the system's working point to extract the maximum output power from the wind turbine. Algorithms such as Perturb and Observe will be implemented in the STM32 microcontroller, which

periodically adjusts the PWM signal and monitors the voltage and current output from the generator to compute power. The microcontroller responds quickly to changes in power to maintain operation at the optimal point, thereby improving the overall efficiency of the system.

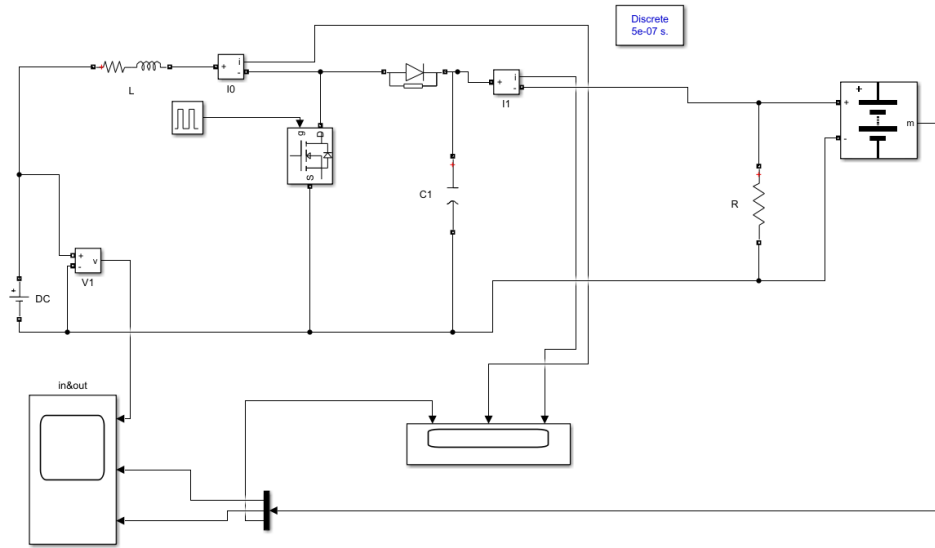


Figure 11: Boost simulation

### 2.3 Charging control

We design a charging control module intelligently adjusts the current delivered to the battery based on its charging state. It encompasses voltage monitoring, overcharge protection, over-discharge protection, and short-circuit protection functionalities. When the battery is fully charged, the system automatically stops charging to prevent overcharging. Conversely, it restricts output when the battery charge drops below a preset threshold to safe guard battery longevity.

The battery charging module is controlled by the function `outVI_cal` that determines the charging mode based on real-time voltage and current measurements obtained through ADC sampling via pins PA2 and PA3. The system compares measured voltage with reference values to select the charging mode, then transmits the mode flag to the boosting module for PWM signal calculation.

Due to implementation complexity, we implemented a two-stage charging approach. In the first stage, when battery voltage is low, the system applies Constant Current (CC) mode at 5A until voltage reaches 44.8V. The second stage switches to Constant Voltage (CV) mode at 48V, maintained until current drops below the 1A termination threshold. These threshold values are preliminary estimates for initial testing.

The design accommodates the vertical axis wind turbine's preset 200W input power. While simpler than three-stage charging, this approach may impact long-term battery

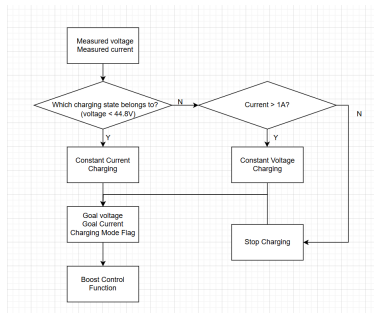


Figure 12: flowchart of charging

health and exhibit suboptimal charging efficiency due to the coarse threshold settings. Future improvements will include refining threshold values through systematic testing, potentially implementing three-stage charging, and optimizing charging power efficiency.

To facilitate user monitoring of the system’s status, we also use an intuitive display interface is designed using an 1.3 inch TFT LCD ???. This screen will show real-time information, such as battery voltage, current output, power status, and operational time. For output and power status, we can directly get

### 2.3.1 interrupt

The charging protection mechanism has been implemented using interrupt-based architecture, including two main functions: `Inter_OCP(int32_t ocpValue)` for output over-current protection and `Inter_OVP(int32_t ovpValue)` for output over-voltage protection.

The protection system activates when either the battery voltage or current exceeds predefined threshold values and the over-limit condition persists for more than 200ms. Upon triggering, the system immediately sets the corresponding protection flag, disables PWM signal output, and completely cuts off voltage and current supply. The state machine then transitions to fault mode, indicated by fault LED illumination, and remains in this state until receiving a RST signal for restart.

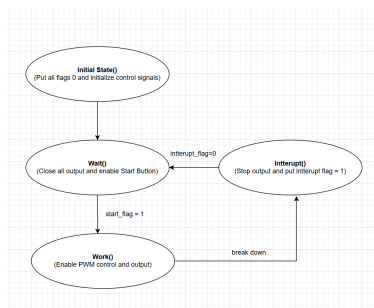


Figure 13: Statemachine

This interrupt-driven approach ensures rapid response to potentially dangerous conditions while maintaining system stability through the state machine architecture 13.

### 3 Verification

As shown in Table 1, we use wind test to verify our design.

Table 1: Wind Turbine Performance Test Results

Test Condition	TSR	Power (W)
9 m/s wind		
9 m/s wind		
9 m/s wind		

#### 3.1 Mechanical part

As the friction occurs, we use 0 load to test if our wind turbine can run under 9 m/s wind conditions. If it can run, we connect the 24 v motor to see the power output.

#### 3.2 Electronic part

We test electronic part separately using a 24v DC power charging a 48V100ah battery, which type is JLLD-DL-48100R. We successfully charge the battery.

## 4 Costs

### 4.1 Cost

Table 2: Material Cost Table from Dec.21th to Apr.13th

Time	Item	Description	Quantity	Price
12/21	HTD 5M	1000, 30	1	30
1/7	Carbon fibre tube	OD 4mm, ID 2mm, L 1m	4	27.24
1/7	Step screw	semi-toothed 6 * 16 * M5	5	9.41
1/9	Kafuter	70g	1	8
2/26	PLA	K5-1.75-WHT-1KG	5	400
3/3	DC Generator	DC 300W	1	200.04
3/6	Screw	M4 * 55	10	2.8
3/6	Nut	M4	100	2.62
3/6	Bearing	32*52*20	2	50
3/11	HTD 5M	3900, 30	2	220
3/11	Al tube	1500*32	4	160
3/12	Bearing	32*52*20	3	67.5
3/17	Bearing	40*62*12	8	34.4
3/18	Carbon fibre tube	OD 4mm, ID 2mm, L 1m	4	27.24
3/26	3-way aluminum corner bracket	30*30*30	16	93.12
3/26	Bearing	Sliding Bearings	4	18.18
3/27	Bearing	51407/P5 35*80 *32	4	95.04
4/8	Aluminum profile	10m	1	330.9

Table 3: Labor Cost Table from Dec.21th to Apr.13th

Task	Hours	Rate (¥/hour)	Price
SolidWorks Designing	30	100	3000
3D Print	6	70	420

Assemble	10	100	1000
PCB Designing	20	100	2000
PCB Debugging	15	100	1500
Documentation	18	50	900

## 4.2 Schedule

Table 4: Schedule Table from Dec.21th to Apr.20th

<b>Week of</b>	<b>Plan</b>	<b>Member</b>
Dec 21, 2024	CFD	C.S.J
Jan 21, 2024	Design blade	C.S.J
Jan 21, 2025	Design base	Y.Y.Z
Feb 20, 2025	1th PCB Designing	J.Y.G J.Y.L
Feb 20, 2025	DC motor choose	Y.Y.Z
Feb 20, 2025	Design pulley	C.S.J
Mar 1, 2025	2th PCB Designing	J.Y.G J.Y.L
Mar 18, 2025	Design connection	Y.Y.Z C.S.J
Mar 20, 2025	PCB debudgging	J.Y.G J.Y.L
Apr 10, 2025	Assemble	Y.Y.Z C.S.J
Apr 10, 2025	3th PCB Designing	J.Y.G J.Y.L

## 5 Conclusion

Energy is the material basis for the existence and development of human society. The development of clean, safe and sustainable energy is the key to addressing future energy demands. This project provides valuable exploration for the development of renewable energy technology by developing a new type of vertical-axis wind turbine (VAWT) and conclusively validates the mechanical concept while identifying clear pathways for electrical system improvements, showing a necessary step in transitioning from laboratory validation to field deployment.

While the completed prototype achieved mechanical stability and operational reliability under test conditions, it fell short of the target power conversion efficiency in real-world wind scenarios. The system currently delivers 50W at optimal conditions (9m/s wind speed, TSR=2), below our 200W target.

Besides, there are still several uncertainties require consideration for future implementation:

- **Efficiency Optimization:** The boost converter circuit exhibits higher-than-expected losses and a narrow range of output voltage and current, limiting VAWTs' applications and working circumstances.
- **Material Fatigue:** While 3D-printed components met 1,000-hour durability targets, long-term wear patterns indicate possible need for reinforced composites

To mitigate these issues, we propose that:

- Redesign the circuit to make its output voltage and current range larger, thereby adapting to more potential application scenarios; Replace electrical components, such as using GaN-based switching components, to reduce losses in boost converter circuit.
- Exploring carbon-fiber reinforcement for high-stress 3D-printed parts.

Although there are certain deficiencies in the current achievements, this design demonstrates a viable path toward decentralized wind energy solutions. From a broader perspective, this research provides new technical options for distributed renewable energy systems. We believe that through continuous optimization, this design is expected to become an important component of the future energy structure, especially in remote areas and microgrid applications. Our work is just a beneficial attempt in the long river of the development of wind power generation technology. It is expected that the subsequent research can achieve greater breakthroughs on this basis and make greater contributions to the cause of clean energy for mankind.

## References

- [1] R. E. Sheldahl and P. C. Klimas, "Aerodynamic characteristics of seven symmetrical airfoil sections through 180-degree angle of attack for use in aerodynamic analysis of vertical axis wind turbines," Sandia National Laboratories, Technical Report, 1981, SAND80-2114, pp. 52–62.
- [2] F. Ponta, J. Seminara, and A. Otero, "On the aerodynamics of variable-geometry oval-trajectory darrieus wind turbines," *Renewable Energy*, vol. 32, no. 1, pp. 35–56, Jan. 2007, Received 5 October 2005; accepted 14 December 2005; available online 9 March 2006, ISSN: 0960-1481. DOI: 10.1016/j.renene.2005.12.002. [Online]. Available: <https://doi.org/10.1016/j.renene.2005.12.002>.
- [3] Ningbo Jiebao Power Transmission Systems Co., Ltd., *Htd 5m tooth profile diagram*, Included in physical product manual, Accessed in April 2025, 2024.
- [4] norelem USA. "Toothed belt profile htd 5m." (2025), [Online]. Available: <https://www.norelemusa.com/en-us/Product-Overview/Systems-and-components-for-machine-and-plant-construction/22000/Toothed-belts-toothed-belt-pulleys/Toothed-belt-profile-HTD-5M/p/agid.18242> (visited on 04/13/2025).

## **Appendix A Example Appendix**

An appendix can go here! Make sure you use the `\label{appendix:a}` above so that you can reference this section in your document.